Letter

Insight into Isomeric Effect on the Photoluminescence and Mechanoluminescence of Cyanostilbene Derivatives

Yuqing Jiang,[‡] Yuhao Shi,[‡] Deping Hu, Qian Peng,* Guangxi Huang,* and Bing Shi Li*

Cite This: *J. Phys. Chem. Lett.* 2022, 13, 7681−7688
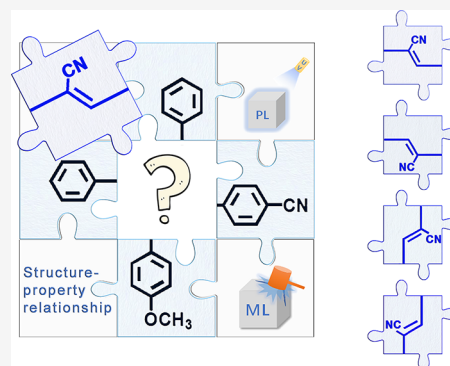
Read Online

ACCESS | ⬛ Metrics & More | 📰 Article Recommendations | SI Supporting Information

ABSTRACT: Molecular structures, packings, and intermolecular interactions significantly affect the photophysical properties of organic luminogens. In this work, the photoluminescence (PL) and mechanoluminescence (ML) of two pairs of isomers, **1/2** and **3/4**, were systematically explored. The fluorescence of crystals **1c** and **4c** is much brighter than that of their isomers **2c** and **3c**, respectively. Only **1c** is ML-active among all four molecules. Single-crystal structural analysis revealed that isomerization of a substituent group affected their molecular packing and intermolecular interactions. Stronger intermolecular interaction and intact three-dimensional hydrogen-bonded networks were formed only in crystal **1c**, which were essential for preventing slippage of molecular layers and generating ML; the other molecules were either lacking $\pi-\pi$ interactions or C−H···π interactions. Theoretical calculation suggested that the energy barrier between the Franck−Condon (FC) structure and minimum energy crossing point (MECP) structure of **2/3** was much lower than that of **1/4**. Nonradiative decay channels of molecules **2** and **3** were thus more easily activated, which led to their lower quantum yield.

As one of the most important functional materials, organic luminescent materials have attracted wide attention for their various potential applications, such as in chemical/biological probes, bioimaging, organic light-emitting diodes (OLEDs), anticounterfeiting, etc.[1−7] Moreover, some organic luminogens are sensitive to external stimuli, including mechanical force, organic compound vapors, temperature, electricity, or light.[8−17] In response to the external stimuli, the photophysical properties of luminogens could be regulated and controlled. Among these luminogens, mechanoluminescent (ML) materials are an interesting type, which can generate a flash of light under mechanical stimuli without photoexcitation. The exploration of organic ML materials has rapidly expanded in the past few years because of their potential applications, such as in lighting, nondestructive stress or crack sensors, anticounterfeiting, smart skin, and so on.[18−21] ML materials with additional room-temperature phosphorescence or thermally activated delayed fluorescence have also been explored.[22−26]

The latest progress in ML materials suggests that the ML property is highly dependent on the molecular configuration and the intermolecular stacking mode in the crystalline state. Strong intermolecular interactions, high molecular dipole moment, or an intact three-dimensional hydrogen-bonded network can facilitate the generation of the ML property. Nevertheless, the development of purely organic ML materials is still in the initial stage and is confronted with multiple challenges: the number of ML-active molecules is quite limited, and a systematic strategy guiding the design of ML-
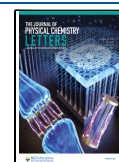
active molecules is missing because of a lack of knowledge regarding the structure−property relationship.[27−31] With respect to the structure−property relationship, substituent position has great influence on the electronic structure, intermolecular interactions, and packing modes; subtle changes in substituent position might lead to dramatically different photophysical properties of the isomers.[32−34] Related research on positional isomers is full of interesting application value for luminogen design. Therefore, development of novel ML-active crystals and deciphering the structure−property relationship are crucial for gaining new insight into the ML mechanism.

We recently reported two ML-active cyanostilbene derivatives and the influences of the type of substituent on the ML property.[35] Herein, we chose two pairs of positional isomers, **1/2** and **3/4**, as the target molecules and obtained a deep insight into the relationship among the structure−PL/ML property (Figure 1). The cyano and methoxyl groups were chosen at the para-position in order to reduce possible conformational variation and simplify the research model. The fluorescence of crystal **1c** (molecules in single-crystal form are denoted as **c**, and it applies to all the other molecules below)
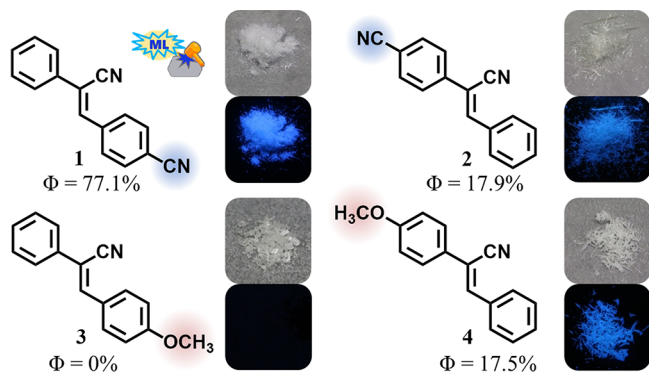
Figure 1. Molecular structures and photos of **1−4**. Photos of single crystals were taken under natural light (upper) and under UV illumination (lower).

and **4c** is much brighter than that of crystal **2c** and **3c**, respectively. It is unexpected that the quantum yield of **3c** is even as low as 0%. Among the four crystals, only **1c** is ML-active. Theoretical results revealed that molecular structure and excited properties determined the photophysical processes of the two pairs of isomers. The crystal structures demonstrated that **1c** and **2c** possessed similar molecular packings. However, the subtle difference in the intermolecular interactions led to dramatically different ML properties of the two crystals, with only crystal **1c** being ML-active. These results of structure−property relationship help to better understand the influence of the different substituent positions on PL and ML.

Compounds **1−4** were obtained according to a simple one-step synthetic process reported in the literature, and their structures were confirmed by NMR spectra (Figures S10−S17).[35−38] As shown in Figure S1, the UV−vis absorption spectra of compounds **1−4** were measured in a dilute THF solution (10 μM). Because of similar functional groups, compounds **1** and **2** exhibited the same maximum absorption peak located at 322 nm; compounds **3** (λ_{abs} = 336 nm) and **4** (λ_{abs} = 331 nm) had slight difference. The presence of an electron-donating methoxyl group increased conjugation and intramolecular charge transfer (ICT) (Figure S2), leading to the red-shift of the absorption peak when compared to that of two cyano-substituted compounds, **1** and **2**.

Single crystals of **1c−4c** could be easily recrystallized from their ethanol solution, and their photophysical properties are summarized in Table S1 and Figure S3. They exhibited the same colorless appearance but distinct fluorescence properties. Needle-like single crystals **1c**, **2c**, and **4c** emitted similar blue fluorescence under UV irradiation (Figure 1), and block single-crystal **3c** was almost nonemissive. **1c** (λ_{em} = 430 nm, Φ_f = 77.1%, τ = 8.537 ns) had obviously higher photoluminescence quantum yield (PLQY) and longer fluorescence lifetime than those of **2c** (λ_{em} = 448 nm, Φ_f = 17.9%, τ = 3.136 ns), while bright **4c** (λ_{em} = 454 nm, Φ_f = 17.5%, τ = 1.342 ns) formed a strong contrast to dark **3c** ($\Phi_f \approx$ 0%).

When **1c** was ground by metal ladle or glass rod under dim light at room temperature, blue emission could be observed (Figure 2a). No ML could be generated in the case of crystals **2c−4c**. The ML maximum of **1c** was at the wavelength of ∼450 nm, which is longer than its PL emission wavelength. ML spectra were always bathochromic compared to the corresponded fluorescence spectra, implying that PL and ML came from different regions of the crystal. Powder X-ray diffraction (PXRD) spectra and differential scanning calorimetry (DSC) of the four crystals were also performed. Samples **1c** and **2c** showed almost the same PXRD patterns (Figure 2b), revealing their highly similar molecular packing as verified
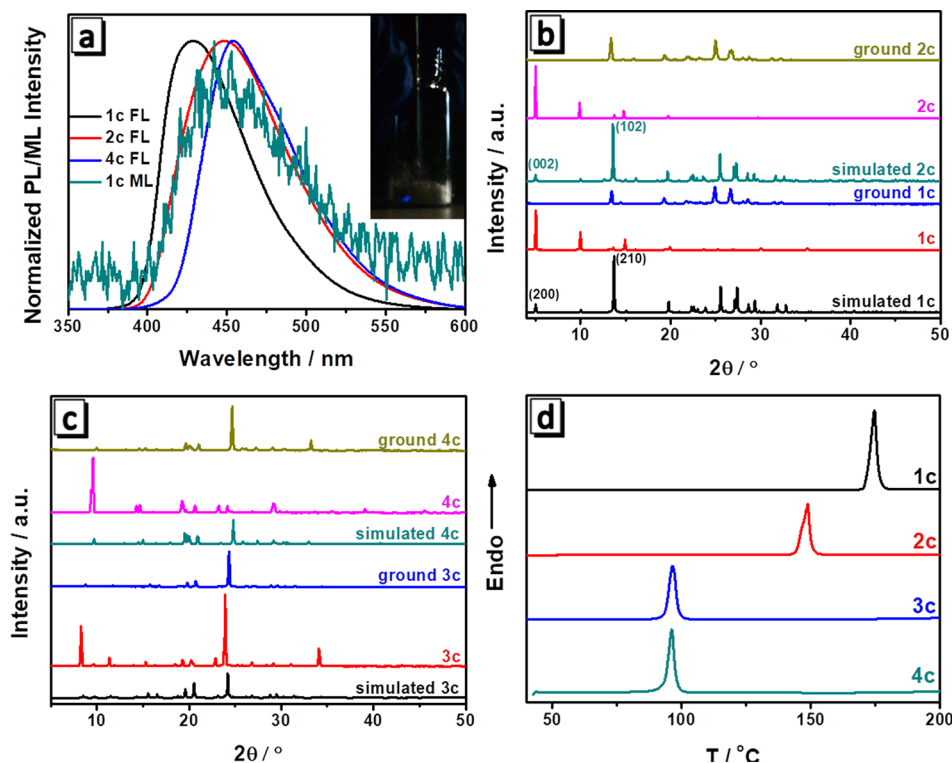

Figure 2. (a) PL spectra of **1c**, **2c**, and **4c** and ML spectrum of **1c**; inset is the ML image of **1c** at room temperature. (b) PXRD patterns of **1c** and **2c** before and after grinding. (c) PXRD patterns of **3c** and **4c** before and after grinding. (d) DSC curves of **1c−4c**.
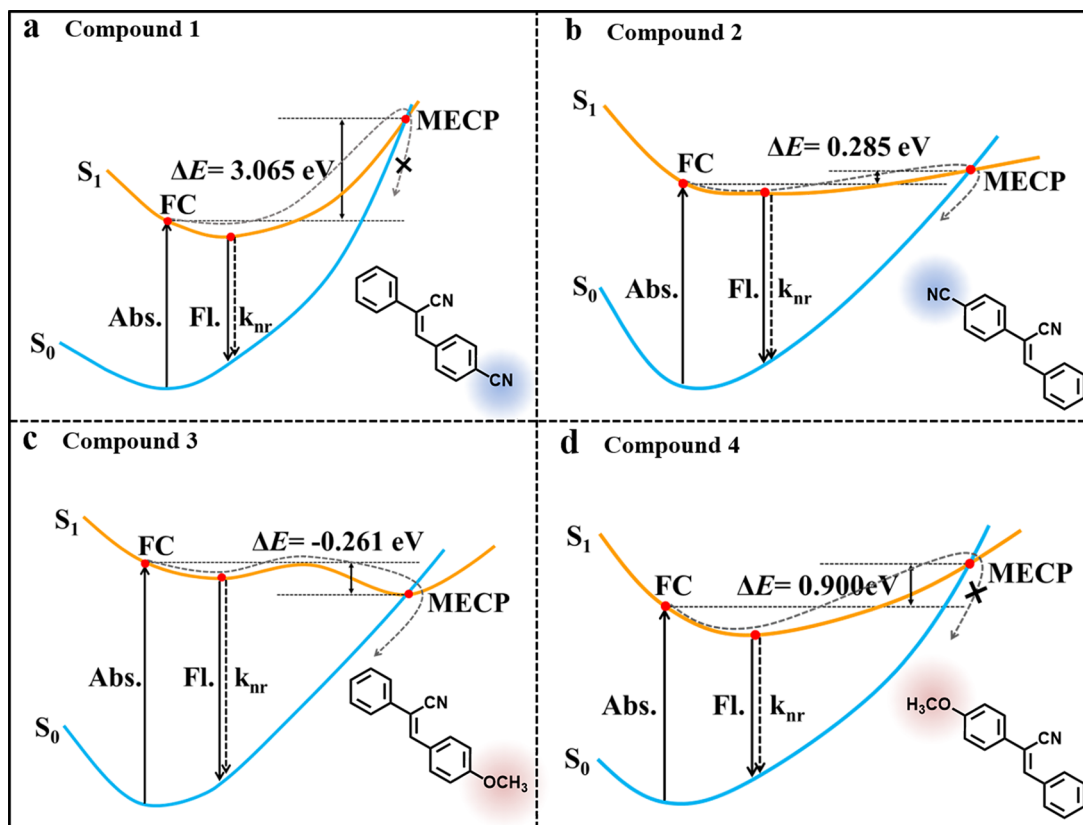
Figure 3. Schematic graph of the two nonradiative decay channels, including the direct harmonic vibrational relaxation and deactivation via MECP structure away from the harmonic region for compounds.

in the following section. After grinding, their PXRD patterns had some changes: the diffraction peaks of **1c** and **2c** at $2\theta =$ 5.01° and 4.99° disappeared, which corresponded to the lattice spacing of d(002) and d(200) planes with a distance of 17.64 and 17.69 Å, respectively. DSC thermograms revealed that **1c** (173.5 °C) had a melting point greater than that of **2c** (148.8 °C) (Figure 2d), which probably implied the existence of stronger intermolecular interaction in **1c**. However, the isomerization of methoxyl group had little influence on the thermal stability of **3c** (96.4 °C) and **4c** (96.1 °C). The PXRD patterns of **3c** and **4c** had similar main peaks at $2\theta =$ 24.2° and 24.8° (Figure 2c), corresponding to the lattice spacings of d(004) and d(200) with the distance of 3.67 and 3.59 Å, respectively. After grinding, their main diffraction peaks in PXRD patterns remained almost the same.

Molecules **1** and **3** are isomeric compounds of **2** and **4**, respectively. However, the fluorescence emission intensity of their crystals was different: the quantum yield of **1c** is more than four times that of **2c**; **4c** emitted bright fluorescence, while **3c** was almost nonemissive. To gain insight into the underlying mechanism for the specific experimental phenomena, theoretical calculation was performed to investigate compounds in the crystalline phase, including potential energy surfaces of the ground and excited states, intermolecular excitonic couplings (J) of the excited states, excited-state decay rates, and so on. Detailed computational information is given in the Supporting Information, and the computational model is shown in Figures S4 and S5. The potential energy surfaces of all the systems were totally examined, including the position of equilibrium geometry in the ground state (S_0) and the excited state (S_1) in the harmonic region (HR) and the minimum-

energy crossing point (MECP) between two electronic states beyond the harmonic region, as shown in Figure 3. It is obvious that there is an MECP with very high energy relative to the equilibrium point for compound **1** (Figure 3a), which suggests that its PLQY is mainly determined by the radiative k_r and nonradiative decay rates k_{nr}^{HR} from the equilibrium position of S_1 in HR with the nonradiative pathway via MECP neglected. In addition, **1c** belongs to J-aggregation with strong excitonic couplings of −89.28 meV (Figure S5 and Table S2), which would increase the transition dipole moment and decrease the excitation energy (Table S3), causing the red shift of fluorescence spectrum and profiting emission. The k_r and k_{nr}^{HR} of compound **1** after considering the excitonic coupling were calculated to be 6.36×10^8 s^{-1} and 2.08×10^8 s^{-1}, respectively, and the resultant PLQY is 75.4%, which is close to the experimental values. There is an energetically accessible S_0/ S_1 MECP for compound **2** (Figure 3b), which indicates that the nonradiative decay via MECP would significantly dissipate the excited-state energy in addition to the radiative and nonradiative decays within HR.[39] Although similar to **1c** in that J-aggregation was formed in **2c**, the PLQY of **2c** is much smaller than that of **1c**. The MECP of **3** is even lower than the equilibrium point of S_1 in energy (Figure 3c), which makes the deactivation channel via MECP favorable thermodynamically, completely quenching the fluorescence as verified by the extremely low PLQY of **3c**. Moreover, the H-aggregation is dominant in **3c** with very large J of 113.15 meV, which always quenches emission. For **4c**, the high energy barrier greatly hampers the nonradiative pathway via MECP (Figure 3d), promoting the PLQY. Moreover, the excitonic couplings in **4c** were relatively weak, with values less than 50 meV, which have
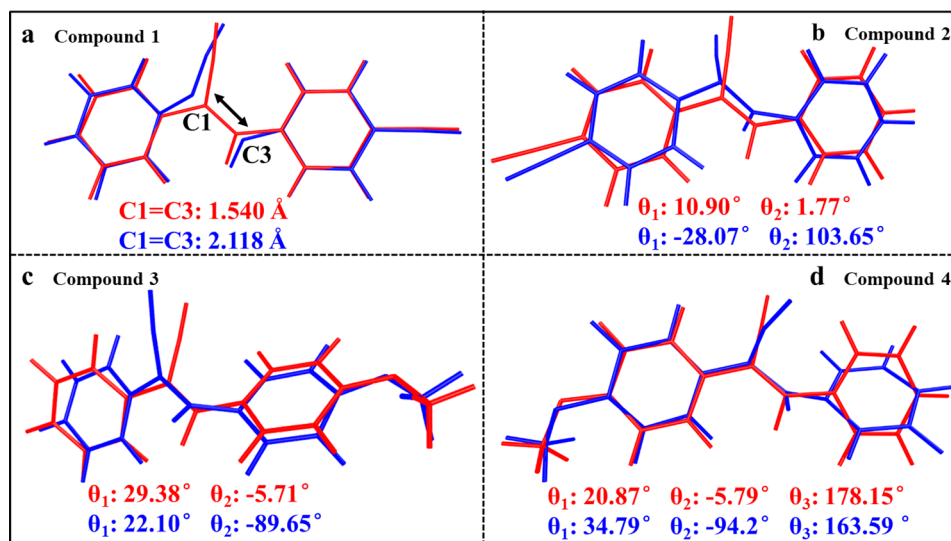
Figure 4. Comparison of key geometrical parameters between S_0 geoemtries (red) and MECP geometries (blue) of compounds (a) **1**, (b) **2**, (c) **3**, and (d) **4**. Definition of angles $\theta_1-\theta_3$ is shown in Figure S6.

Table 1. Summary of the Intermolecular Interactions in Four Single Crystals

crystal	1c	2c	3c		4c	
conformation			gray	blue	gray	blue
	d (Å)	d (Å)	d (Å)	d (Å)	d (Å)	d (Å)
C−H···O			2.735(2)[a]	2.806(2)	2.495(1)	2.495(1)
			2.967(2)	2.895(2)	2.524(1)	2.524(1)
					2.661(1)	2.661(1)
					3.113(1)	3.113(1)
C−H···N	2.549(4)	2.476(2)	2.681(1)	2.681(1)	2.617(1)	2.617(1)
	2.564(2)	2.675(2)	2.786(2)	2.732(2)	2.741(1)	2.741(1)
	2.628(1)	2.695(2)	2.789(2)	2.824(2)	2.762(1)	2.762(1)
	2.643(1)	2.776(2)	2.800(2)	2.923(2)	2.848(1)	2.848(1)
	2.658(1)	2.985(2)	3.102(1)	3.102(1)	2.992(1)	2.992(1)
	2.684(1)				3.014(1)	3.014(1)
					3.027(1)	3.027(1)
					3.073(1)	3.073(1)
					3.080(1)	3.080(1)
					3.089(1)	3.089(1)
$\pi-\pi$[b]	3.332(2)	3.388(2)				
	3.359(2)	3.408(2)				
C−H···π	2.877(2)		2.715(1)	2.715(1)	2.754(1)	2.754(1)
			2.732(1)	2.732(1)	2.784(1)	2.784(1)
			2.773(1)	2.773(1)	2.899(1)	2.817(2)
			2.854(1)	2.854(1)	2.914(2)	2.860(2)
			2.870(1)	2.870(1)	2.920(1)	2.899(1)
			2.872(1)	2.872(1)		2.920(1)
			2.893(1)	2.893(1)		
			3.122(1)	3.122(1)		

[a]The number of hydrogen bonds. [b]$\pi-\pi$ interaction between phenyl ring and vinyl unit.

little effect on emission. Therefore, the PLQY of **4c** is much higher than that of **3c**.

To establish the structure−property relationship, the detailed analyses of geometrical structures at the different key points are given in Figures 4 and S6 and Table S4. There is a slight variation between the S_0 geometry and S_1 geometry among the four compounds, which suggests their k_{nr}^{HR} values are very small. The geometrical structures at the MECP (MECP geometry) exhibit more obvious change compared to those S_0 geometries for the four compounds. For compound **1**, the C=C double bond is almost broken with the bond length increasing from 1.540 Å in S_0 geometry to 2.118 Å in the MECP structure (Figure 4a), which differs from that occurring in the rigid solid-phase environment, as seen by the high energy barrier in Figure 3. As a result, compound **1** emits bright light in crystal form. As shown in Figure 4b, the main changes for compound **2** are the twisting of the dihedral angles of the central fragment between the two phenyl rings, which is

less affected by the external environment and would occur at a relatively smaller energy barrier. This process causes one more nonradiative pathway, decreasing the PLQY of compound **2**. For compound **3**, only the central dihedral angle changes (Figure 4c), which occurs easily even without the influence of the external environment. As a consequence, the nonradiative decay via MECP becomes dominant and causes the fluorescence quenching in the crystalline phase. Compared with compound **3**, more significant changes from S_0 geoemtry to MECP geometry occur in compound **4** (Figure 4d), which leads to a bit higher energy barrier uphill to MECP, and the fluorescence can be observed in compound **4**.

Since the molecular packing plays a key role in the photophysical properties of single crystals, the corresponding crystal structures were then investigated in detail. The single-crystal data of **1c**−**4c** are listed in Table S5. Crystal **1c** and **3c** belong to the orthorhombic system with a centrosymmetric *Pnma* and noncentrosymmetric *Pna*2$_1$ space group, respectively. For **2c**, the molecules exhibit a monoclinic system with the space group of centrosymmetric *P*2$_1$/*c*, while **4c** belongs to a triclinic system with a centrosymmetric *P*$\bar{1}$ space group. Molecules in the unit cell of **1c** or **2c** only showed one conformation (Figure S7a,b), while both **3c** and **4c** had two different conformations (gray and blue) (Figure S7c,d). To explore the structure−property relationship, intermolecular interactions in single-crystal **1c**−**4c** were carefully analyzed. The intermolecular hydrogen bonds shorter than 3.2 Å are listed in Table 1. Each molecule in crystal **1c** interacted with six neighboring molecules through 6 + 1 types of (total of 10 + 2) weak hydrogen bonds (C−H···N + C−H···π) with distances ranging from 2.549 to 2.877 Å (Figures 5a and S8a,b). Besides, strong π−π interactions were present between neighboring molecules in the upper and lower layers (Figure 5b). Because of the existence of relative slippage, there are π−π interactions between the central vinyl group of one molecule

and the phenyl ring of another molecule. There were 2 types of π−π interactions (total of 4) with short distance (3.332 and 3.359 Å) for every molecule **1** in total (Figure S8c). Compared to isomer **1**, crystal **2c** had no C−H···π interactions but similar C−H···N and π−π interactions (Figure 5c). There were 5 types of C−H···N interactions (total of 10) with distances ranging from 2.476 to 2.985 Å (Figure S8d and S8e). The distance of π−π interactions in **2c** (3.388 and 3.408 Å) is slightly longer than those in **1c** (Figures 5d and S8f). In crystal **3c** and **4c**, dihedral angles between the phenyl ring and central vinyl group range from 24.27° to 32.23°, which caused large tortuosity of their conformations. As a result, π−π interactions between neighboring molecules in upper and lower layers were replaced by C−H···π interactions. For crystal **3c**, each gray and blue conformation interacted with ten neighboring molecules (Figure 5e,f). The gray conformation possessed 2 types of C−H···O bonds (2.735 and 2.967 Å) (total of 4), 5 types of C−H···N bonds (2.681−3.102 Å) (total of 10), and 8 types of C−H···π bonds (2.715−3.122 Å) (total of 8) (Figure S9a). The same types and numbers of C−H···O (2.806−2.895 Å), C−H···N (2.681−3.102 Å), and C−H···π (2.715−3.122 Å) interactions were observed for the blue conformation (Figure S9b). For crystal **4c**, each molecule in gray and blue conformations interacted with nine and ten neighboring molecules through multiple hydrogen bonds (Figure S9c,d), respectively.[35] There were 20 (4 + 10 + 6) and 22 (4 + 10 + 8) weak hydrogen bonds (C−H···O + C−H···N + C−H···π) with distances ranging from 2.495 to 3.113 Å related to gray and blue conformations (Figure S9e,f), respectively.[35]

Among the four crystals, only crystal **1c** was ML-active. According to our previous paper,[35] we considered the deficiency of π−π interactions caused the ML inactivity of **4c**, which also could be applied to that of **3c**. π−π interactions could restrict the rotation of phenyl groups or the relative slippage of molecules in neighboring layers, which would decrease the nonradiative relaxation of the excited state induced by mechanical stimulus during the fracturing process of the crystal. As a pair of isomers, **1** and **2** displayed very similar packing mode though they belonged to different space groups (Figure 6), which provided great convenience for us to elucidate the molecular packing−ML property relationship. As shown in the blue circle in Figure 6b,d, every two piles of molecules **1**/**2** formed through C−H···N interactions and π−π stacking arranged into a herringbone structure with neighboring two piles of molecules at a certain angle. Phenyl rings of **1** in the red circle interacted with adjacent ones by C−H···π interactions (Figure 6a,b), resulting in an intact three-dimensional hydrogen-bonding network. In contrast, there were no interactions between adjacent phenyl rings of **2** in the black circle (Figure 6c,d), which made these molecules only form a two-dimensional hydrogen-bonding network. The lack of intermolecular interactions in one dimension probably caused its lower melting point. Additional information could be obtained from the aforementioned PXRD patterns. There existed the same characteristic diffraction peaks at $2\theta = 5.0°$ in the PXRD pattern of **1c** and **2c**, which were attributed to the lattice spacing of the d(200) (17.64 Å) and d(002) (17.69 Å) planes, respectively. The distance of 17.64 Å corresponded with the width of two piles of molecules of **1** formed through C−H···N interactions and π−π stacking (along the *c*-axis), while 17.69 Å correlated with the width of two piles of molecules of **2** formed through C−H···N interactions and π−π stacking (along the *b*-axis). After grinding, disappearance of the
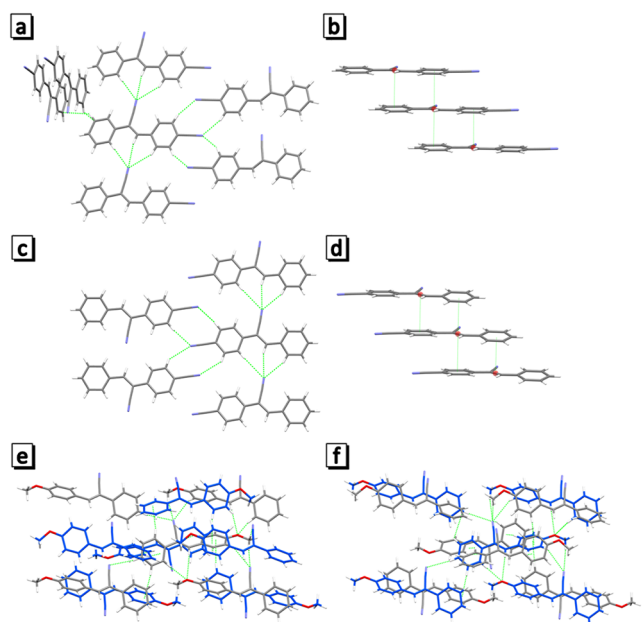

Figure 5. (a) C−H···N and C−H···π interactions in crystal **1c**. (c) C−H···N interactions in crystal **2c**. π−π interactions in crystal (b) **1c** and (d) **2c**. Centroids of vinyl groups are shown in red. C−H···O, C−H···N, and C−H···π interactions related to (e) gray and (f) blue conformation in crystal **3c**.
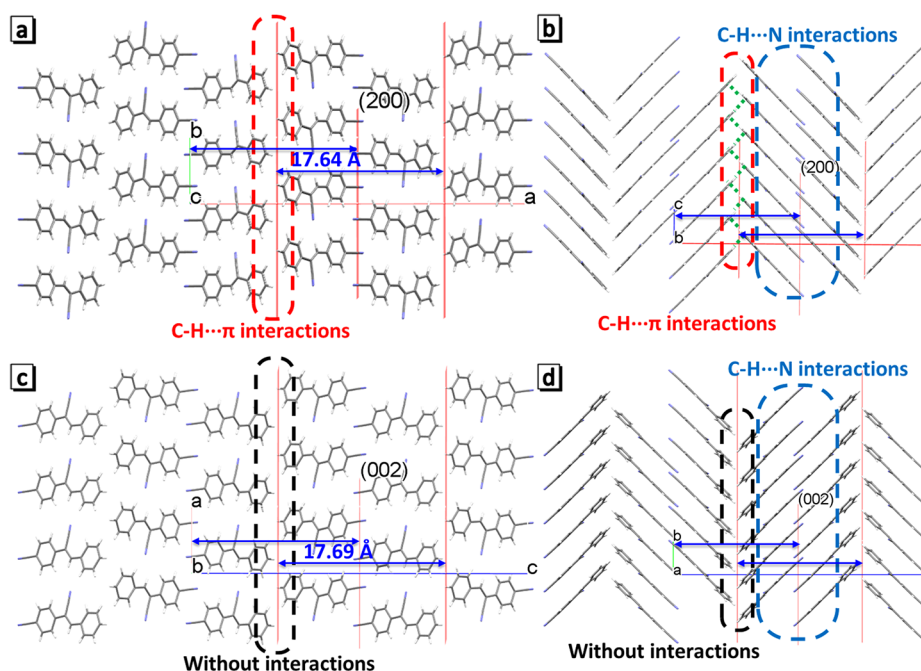
Figure 6. Molecular packing mode in **1c** viewed from (a) *c*-axis and (b) *b*-axis. The molecular packing mode in **2c** viewed from (c) *b*-axis and (d) *a*-axis. Green line in panel b indicates the additional C−H···π interactions in **1c**.

diffraction peaks at $2\theta = 5.0°$ occurred, implying that the corresponding planes had been destroyed. A similar molecular packing and fracture mode could be found from the crystal structures of **1c** and **2c**, and the obvious difference is the absence/presence of C−H···π interactions and intact three-dimensional hydrogen-bonding network. According to the above analysis, our deduction was as follows: When **1c** was ground, fractures of crystals occurred along the plane in the red circle and C−H···π interactions were destroyed. The disappearing interactions probably caused charge/energy redistribution and excited the molecules into an excited state through a somewhat different mechanism. In contrast, when **2c** was crushed, the fracture of crystals occurred along the plane in the black circle, but no intermolecular interactions were destroyed. Thus, no energy could be utilized to excite the molecules to realize bright ML. These results proved once more the significance of a three-dimensional hydrogen-bonded network for the ML phenomenon.[40]

In summary, the isomeric effect on the PL and ML properties of two pairs of cyanostilbene isomers, **1**/**2** and **3**/**4**, was systematically investigated. The fluorescence of **1c** and **4c** is obviously brighter than that of **2c** and **3c**, respectively. Specifically, the quantum yield of **3c** is even as low as 0%, and only **1c** is ML-active among four crystals. Theoretical calculations indicated that the energy barrier between the FC structure and MECP structure of **2**/**3** was much lower than that of **1**/**4**, respectively, which activated the nonradiative decay channels and led to lower PLQY. Single-crystal structure analysis revealed that **3c** and **4c** were lacking π−π interactions, probably resulting in their ML inactivity. Although **2c** displayed a packing mode very similar to that of **1c**, the deficiency of additional C−H···π interactions causes its incomplete hydrogen-bonded network. Therefore, only **1c** displays the ML phenomenon.

■ ASSOCIATED CONTENT

Ⓢ **Supporting Information**

The Supporting Information is available free of charge at https://pubs.acs.org/doi/10.1021/acs.jpclett.2c01866.

Detailed characterization of four molecules, absorption spectra, photophysical properties, DFT calculations, single crystal data, and intermolecular interactions analysis (PDF)

Crystallographic data for **1c** (CIF)

Crystallographic data for **2c** (CIF)

Crystallographic data for **3c** (CIF)

■ AUTHOR INFORMATION

Corresponding Authors

Qian Peng − *Institute of Chemistry, Chinese Academy of Sciences, Beijing 100190, China;* Ⓘ orcid.org/0000-0001-8975-8413; Email: qpeng@iccas.ac.cn

Guangxi Huang − *Key Laboratory of New Lithium-Ion Battery and Mesoporous Material, College of Chemistry and Environmental Engineering, Shenzhen University, Shenzhen 518055, China;* Ⓘ orcid.org/0000-0002-9064-3047; Email: huanggx@iccas.ac.cn

Bing Shi Li − *Key Laboratory of New Lithium-Ion Battery and Mesoporous Material, College of Chemistry and Environmental Engineering, Shenzhen University, Shenzhen 518055, China;* Ⓘ orcid.org/0000-0002-0530-0294; Email: phbingsl@szu.edu.cn

Authors

Yuqing Jiang − *Key Laboratory of New Lithium-Ion Battery and Mesoporous Material, College of Chemistry and Environmental Engineering, Shenzhen University, Shenzhen 518055, China*

Yuhao Shi − *Institute of Chemistry, Chinese Academy of Sciences, Beijing 100190, China*

Deping Hu − *Department of Chemistry, University of Rochester, Rochester, New York 14627, United States*

Author Contributions

‡Y.J. and Y.S. contributed equally to this work.

Notes

The authors declare no competing financial interest.

◼ REFERENCES

(1) Liang, J.; Tang, B. Z.; Liu, B. Specific light-up bioprobes based on AIEgen conjugates. *Chem. Soc. Rev.* **2015**, *44*, 2798−2811.

(2) Wang, X.-d.; Wolfbeis, O. S.; Meier, R. J. Luminescent probes and sensors for temperature. *Chem. Soc. Rev.* **2013**, *42*, 7834−7869.

(3) Zhong, C.; Duan, C.; Huang, F.; Wu, H.; Cao, Y. Materials and Devices toward Fully Solution Processable Organic Light-Emitting Diodes. *Chem. Mater.* **2011**, *23*, 326−340.

(4) Zhang, D.-W.; Li, M.; Chen, C.-F. Recent advances in circularly polarized electroluminescence based on organic light-emitting diodes. *Chem. Soc. Rev.* **2020**, *49*, 1331−1343.

(5) Fang, X.; Zheng, Y.; Duan, Y.; Liu, Y.; Zhong, W. Recent Advances in Design of Fluorescence-Based Assays for High-Throughput Screening. *Anal. Chem.* **2019**, *91*, 482−504.

(6) Abdollahi, A.; Roghani-Mamaqani, H.; Razavi, B.; Salami-Kalajahi, M. Photoluminescent and Chromic Nanomaterials for Anticounterfeiting Technologies: Recent Advances and Future Challenges. *ACS Nano* **2020**, *14*, 14417−14492.

(7) Zhou, J.; Liu, Q.; Feng, W.; Sun, Y.; Li, F. Upconversion Luminescent Materials: Advances and Applications. *Chem. Rev.* **2015**, *115*, 395−465.

(8) Roy, S.; Hazra, A.; Bandyopadhyay, A.; Raut, D.; Madhuri, P. L.; Rao, D. S. S.; Ramamurty, U.; Pati, S. K.; Krishna Prasad, S.; Maji, T. K. Reversible Polymorphism, Liquid Crystallinity, and Stimuli-Responsive Luminescence in a Bola-amphiphilic π-System: Structure−Property Correlations Through Nanoindentation and DFT Calculations. *J. Phys. Chem. Lett.* **2016**, *7*, 4086−4092.

(9) Roy, B.; Reddy, M. C.; Jose, G. P.; Niemeyer, F. C.; Voskuhl, J.; Hazra, P. All in One: Stimuli-Responsive, Efficient Mitotracking, and Single Source White Light Emission. *J. Phys. Chem. Lett.* **2021**, *12*, 1162−1168.

(10) Dou, C.; Han, L.; Zhao, S.; Zhang, H.; Wang, Y. Multi-Stimuli-Responsive Fluorescence Switching of a Donor−Acceptor π-Conjugated Compound. *J. Phys. Chem. Lett.* **2011**, *2*, 666−670.

(11) Huang, G.; Jiang, Y.; Yang, S.; Li, B. S.; Tang, B. Z. Multistimuli Response and Polymorphism of a Novel Tetraphenylethylene Derivative. *Adv. Funct. Mater.* **2019**, *29*, 1900516.

(12) Huang, G.; Xia, Q.; Huang, W.; Tian, J.; He, Z.; Li, B. S.; Tang, B. Z. Multiple Anti-Counterfeiting Guarantees from a Simple Tetraphenylethylene Derivative − High-Contrasted and Multi-State Mechanochromism and Photochromism. *Angew. Chem., Int. Ed.* **2019**, *58*, 17814−17819.

(13) Ma, Z.; Wang, Z.; Meng, X.; Ma, Z.; Xu, Z.; Ma, Y.; Jia, X. A Mechanochromic Single Crystal: Turning Two Color Changes into a Tricolored Switch. *Angew. Chem., Int. Ed.* **2016**, *55*, 519−522.

(14) Dong, Y.; Xu, B.; Zhang, J.; Tan, X.; Wang, L.; Chen, J.; Lv, H.; Wen, S.; Li, B.; Ye, L.; et al. Piezochromic Luminescence Based on the Molecular Aggregation of 9,10-Bis((E)-2-(pyrid-2-yl)vinyl)-anthracene. *Angew. Chem., Int. Ed.* **2012**, *51*, 10782−10785.

(15) Qi, Q.; Li, C.; Liu, X.; Jiang, S.; Xu, Z.; Lee, R.; Zhu, M.; Xu, B.; Tian, W. Solid-State Photoinduced Luminescence Switch for Advanced Anticounterfeiting and Super-Resolution Imaging Applications. *J. Am. Chem. Soc.* **2017**, *139*, 16036−16039.

(16) Hu, D.; Zhang, T.; Li, S.; Yu, T.; Zhang, X.; Hu, R.; Feng, J.; Wang, S.; Liang, T.; Chen, J. Ultrasensitive reversible chromophore reaction of BODIPY functions as high ratio double turn on probe. *Nat. Commun.* **2018**, *9*, 362.

(17) Feng, J.; Tian, K.; Hu, D.; Wang, S.; Li, S.; Zeng, Y.; Li, Y.; Yang, G. A Triarylboron-Based Fluorescent Thermometer: Sensitive Over a Wide Temperature Range. *Angew. Chem., Int. Ed.* **2011**, *50*, 8072−8076.

(18) Wang, C.; Yu, Y.; Yuan, Y.; Ren, C.; Liao, Q.; Wang, J.; Chai, Z.; Li, Q.; Li, Z. Heartbeat-Sensing Mechanoluminescent Device Based on a Quantitative Relationship between Pressure and Emissive Intensity. *Matter* **2020**, *2*, 181−193.

(19) Xie, Y.; Li, Z. Triboluminescence: Recalling Interest and New Aspects. *Chem.* **2018**, *4*, 943−971.

(20) Xie, Y.; Li, Z. The development of mechanoluminescence from organic compounds: breakthrough and deep insight. *Mater. Chem. Front.* **2020**, *4*, 317−331.

(21) Li, W.; Huang, Q.; Mao, Z.; Li, Q.; Jiang, L.; Xie, Z.; Xu, R.; Yang, Z.; Zhao, J.; Yu, T.; et al. Alkyl Chain Introduction: In Situ Solar-Renewable Colorful Organic Mechanoluminescence Materials. *Angew. Chem., Int. Ed.* **2018**, *57*, 12727−12732.

(22) Li, J.-A.; Song, Z.; Chen, Y.; Xu, C.; Li, S.; Peng, Q.; Shi, G.; Liu, C.; Luo, S.; Sun, F.; et al. Colour-tunable dual-mode afterglows and helical-array-induced mechanoluminescence from AIE enantiomers: Effects of molecular arrangement on formation and decay of excited states. *Chem. Eng. J.* **2021**, *418*, 129167.

(23) Li, J.-A.; Zhou, J.; Mao, Z.; Xie, Z.; Yang, Z.; Xu, B.; Liu, C.; Chen, X.; Ren, D.; Pan, H.; et al. Transient and Persistent Room-Temperature Mechanoluminescence from a White-Light-Emitting AIEgen with Tricolor Emission Switching Triggered by Light. *Angew. Chem., Int. Ed.* **2018**, *57*, 6449−6453.

(24) Li, W.; Huang, Q.; Yang, Z.; Zhang, X.; Ma, D.; Zhao, J.; Xu, C.; Mao, Z.; Zhang, Y.; Chi, Z. Activating Versatile Mechanoluminescence in Organic Host−Guest Crystals by Controlling Exciton Transfer. *Angew. Chem., Int. Ed.* **2020**, *59*, 22645−22651.

(25) Mu, Y.; Yang, Z.; Chen, J.; Yang, Z.; Li, W.; Tan, X.; Mao, Z.; Yu, T.; Zhao, J.; Zheng, S.; et al. Mechano-induced persistent room-temperature phosphorescence from purely organic molecules. *Chem. Sci.* **2018**, *9*, 3782−3787.

(26) Zhang, X.; Du, L.; Zhao, W.; Zhao, Z.; Xiong, Y.; He, X.; Gao, P. F.; Alam, P.; Wang, C.; Li, Z.; et al. Ultralong UV/mechano-excited room temperature phosphorescence from purely organic cluster excitons. *Nat. Commun.* **2019**, *10*, 5161.

(27) Miao, J.; Zhang, Y.; Zhang, M. Simple anthracene derivatives: different mechanoluminescence properties tailored only by a thiophene group. *Mater. Chem. Front.* **2021**, *5*, 6865−6872.

(28) Yu, Y.; Fan, Y.; Wang, C.; Wei, Y.; Liao, Q.; Li, Q.; Li, Z. Phenanthroimidazole derivatives with minor structural differences: crystalline polymorphisms, different molecular packing, and totally different mechanoluminescence. *J. Mater. Chem. C* **2019**, *7*, 13759−13763.

(29) Yang, J.; Gao, X.; Xie, Z.; Gong, Y.; Fang, M.; Peng, Q.; Chi, Z.; Li, Z. Elucidating the Excited State of Mechanoluminescence in Organic Luminogens with Room-Temperature Phosphorescence. *Angew. Chem., Int. Ed.* **2017**, *56*, 15299−15303.

(30) Yang, J.; Qin, J.; Geng, P.; Wang, J.; Fang, M.; Li, Z. Molecular Conformation-Dependent Mechanoluminescence: Same Mechanical Stimulus but Different Emissive Color over Time. *Angew. Chem., Int. Ed.* **2018**, *57*, 14174−14178.

(31) Yang, J.; Ren, Z.; Xie, Z.; Liu, Y.; Wang, C.; Xie, Y.; Peng, Q.; Xu, B.; Tian, W.; Zhang, F.; et al. AIEgen with Fluorescence−Phosphorescence Dual Mechanoluminescence at Room Temperature. *Angew. Chem., Int. Ed.* **2017**, *56*, 880−884.

(32) Dong, L.; Shang, G.; Shi, J.; Zhi, J.; Tong, B.; Dong, Y. Effect of Substituent Position on the Photophysical Properties of Triphenyl-pyrrole Isomers. *J. Phys. Chem. C* **2017**, *121*, 11658−11664.

(33) Li, J.; Shan, T.; Yao, M.; Gao, Y.; Han, X.; Yang, B.; Lu, P. The effect of different binding sites on the optical and electronic properties of tetraphenylethylene-substituted thiophene isomers. *J. Mater. Chem. C* **2017**, *5*, 2552−2558.

(34) Zhuang, Z.; Bu, F.; Luo, W.; Peng, H.; Chen, S.; Hu, R.; Qin, A.; Zhao, Z.; Tang, B. Z. Steric, conjugation and electronic impacts on the photoluminescence and electroluminescence properties of luminogens based on phosphindole oxide. *J. Mater. Chem. C* **2017**, *5*, 1836−1842.

(35) Huang, G.; Chang, X.; Jiang, Y.; Lin, B.; Li, B. S.; Tang, B. Z. Multi-stimuli responsive cyanostilbene derivatives: pH, amine vapor sensing and mechanoluminescence. *Mater. Chem. Front.* **2020**, *4*, 1720−1728.

(36) Meyers, M. J.; Sun, J.; Carlson, K. E.; Marriner, G. A.; Katzenellenbogen, B. S.; Katzenellenbogen, J. A. Estrogen Receptor-β Potency-Selective Ligands: Structure−Activity Relationship Studies of Diarylpropionitriles and Their Acetylene and Polar Analogues. *J. Med. Chem.* **2001**, *44*, 4230−4251.

(37) Perin, N.; Rep, V.; Sović, I.; Juričić, Š.; Selgrad, D.; Klobučar, M.; Pržulj, N.; Gupta, C. L.; Malod-Dognin, N.; Pavelić, S. K.; et al. Antiproliferative activity and mode of action analysis of novel amino and amido substituted phenantrene and naphtho[2,1-b]thiophene derivatives. *Eur. J. Med. Chem.* **2020**, *185*, 111833.

(38) Krishnan, S.; Miller, R. M.; Tian, B.; Mullins, R. D.; Jacobson, M. P.; Taunton, J. Design of Reversible, Cysteine-Targeted Michael Acceptors Guided by Kinetic and Computational Analysis. *J. Am. Chem. Soc.* **2014**, *136*, 12624−12630.

(39) Ou, Q.; Peng, Q.; Shuai, Z. Toward Quantitative Prediction of Fluorescence Quantum Efficiency by Combining Direct Vibrational Conversion and Surface Crossing: BODIPYs as an Example. *J. Phys. Chem. Lett.* **2020**, *11*, 7790−7797.

(40) Huang, G.; Jiang, Y.; Wang, J.; Li, Z.; Li, B. S.; Tang, B. Z. The influence of intermolecular interactions and molecular packings on mechanochromism and mechanoluminescence − a tetraphenyl-ethylene derivative case. *J. Mater. Chem. C* **2019**, *7*, 12709−12716.

▢▢ Recommended by ACS